New perspectives in silicon micro and nanophotonics

M. Casalino Istituto per la Microelettronica e Microsistemi (IMM) Consiglio Nazionale delle Ricerche, Via P. Castellino n. 111, Napoli, Italy

G. Coppola Istituto per la Microelettronica e Microsistemi (IMM) Consiglio Nazionale delle Ricerche, Via P. Castellino n. 111, Napoli, Italy

L. De Stefano Istituto per la Microelettronica e Microsistemi (IMM) Consiglio Nazionale delle Ricerche, Via P. Castellino n. 111, Napoli, Italy

A. Caliò Istituto per la Microelettronica e Microsistemi (IMM) Consiglio Nazionale delle Ricerche, Via P. Castellino n. 111, Napoli, Italy

I. Rea Istituto per la Microelettronica e Microsistemi (IMM) Consiglio Nazionale delle Ricerche, Via P. Castellino n. 111, Napoli, Italy

V. Mocella Istituto per la Microelettronica e Microsistemi (IMM) Consiglio Nazionale delle Ricerche, Via P. Castellino n. 111, Napoli, Italy

P. Dardano Istituto per la Microelettronica e Microsistemi (IMM) Consiglio Nazionale delle Ricerche, Via P. Castellino n. 111, Napoli, Italy

S. Romano Istituto per la Microelettronica e Microsistemi (IMM) Consiglio Nazionale delle Ricerche, Via P. Castellino n. 111, Napoli, Italy

S. Rao Università degli Studi "Mediterranea", Dipartimento di Ingegneria dell'Informazione, delle Infrastrutture e dell'Energia Sostenibile (DIIES), Via Graziella Loc. Feo di Vito, 89122 Reggio Calabria, Italy

I. Rendina Istituto per la Microelettronica e Microsistemi (IMM) Consiglio Nazionale delle Ricerche, Via P. Castellino n. 111, Napoli, Italy

In the last two decades, there has been growing interest in silicon-based photonic devices for many optical applications: telecommunications, interconnects and biosensors. In this work, an advance overview of our results in this field is presented. Proposed devices allow overcoming silicon intrinsic drawbacks limiting its application as a photonic substrate. Taking advantages of both non-linear and linear effects, size reduction at nanometric scale and new two-dimensional emerging materials, we have obtained a progressive increase in device performance along the last years. In this work we show that a suitable design of a thin photonic crystal slab realized in silicon nitride can exhibit a very strong field enhancement. This result is very promising for all photonic silicon devices based on nonlinear phenomena. Moreover we report on the fabrication and characterization of silicon photodetectors working at near-infrared wavelengths based on the internal photoemission absorption in a Schottky junction. We show as an increase in device performance can be obtained by coupling light into both micro-resonant cavity and waveguiding structures. In addition, replacing metal with graphene in a Schottky junction, a further improve in PD performance can be achieved. Finally, silicon-based microarray for biomedical applications, are reported. Microarray of porous silicon Bragg reflectors on a crystalline silicon substrate have been realized using a technological process based on standard photolithography and electrochemical anodization of the silicon. Our insights show that silicon is a promising platform for the integration of various optical functionalities on the same chip opening new frontiers in the field of low-cost silicon micro and nanophotonics.
[DOI: http://dx.doi.org/10.2971/jeos.2015.15029i]

Keywords: Silicon, photodetector, photonic crystals, surface plasmon polaritons, biosensor

1 INTRODUCTION

Silicon (Si) photonics, at both micro- and nano-metric scale, is a technology for implementing various optical functionalities in silicon, offering the potential for largescale integration of multiple optical and electronic functions on a single silicon chip. This should result in revolutionizing applications in microelectronics in telecommunications (integrated optical circuits), and in biological and chemical sensing. Significant advantages exist when using silicon as the base material for such devices: in particular, the vast amount of research now available to designers and process engineers on all aspects of the material system, as well as the established, global silicon processing industry that has evolved from almost six decades of silicon-based microelectronics fabrication. Silicon wafers have the lowest cost per unit area and the highest crystal quality of any semiconductor material. The industry is able to produce microprocessors with hundreds of millions of components all

Invited ms. received February 17, 2015; revised ms. received May 28, 2015; published June 17, 2015 ISSN 1990-2573

integrated onto thumb-sized chips and offers them at such low prices that they are increasingly used in consumer electronics. Silicon manufacturing represents the most spectacular convergence of technological sophistication and economics of scale [1, 2].

Silicon photonics was pioneered by Soref during the 1980 [3]–[6]. Creating low-cost photonics for mass-market applications by exploiting the powerful IC industry has been the traditional motivation of silicon photonics researchers. Silicon is used in photonics due to its good optical properties, the low cost of the material and its easy manufacturability; at present, however, it is not suitable for the manufacture of active devices. Despite the success of hybrid technologies in achieving active optical components, many people think that only all-silicon active devices will make silicon photonics a "killer technology". Following this line of reasoning, tremendous progress has recently been made in technological processes based on the use of silicon substrates, which has permitted to get reliable and effective fully CMOS-compatible optical components and sensors [7]–[15].

In this paper we have summarized our recent results devoted to increase the performance of both optical silicon devices (guiding structures, high quality factor systems and photodetectors) and sensors for biomedical applications.

2 FANO RESONANCES IN DIELECTRIC NEGATIVE REFRACTING PHOTONIC CRYSTALS

Usually Photonic Crystals (PhCs) are exploited for their band gap proprieties for devices as waveguides, resonant cavity or multiplexing [16]–[18]. A more recent develop of applications of this material has been opened by negative refraction behaviour [19, 20]. Properly choosing the lattice parameter, a, and the hole radius r of a silicon ($\epsilon = 11.9$) based PhC slab, an effective refractive index $n_{\text{eff}} = -1$ is obtained, i.e. opposite to the air index. In this case, an incident k-vector coming from the air, strongly couples with the PhC lattice and a deep resonance appears in the reflectance spectrum. Resonances in reflection spectrum of a PhCs have been used to reconstruct experimentally band structure [21] and Equi Frequency Surface (EFS) [22], but they are very attracting in biosensing application for the strong field enhancement and the radiation confinement. Indeed, in this case negative PhCs are able to trap and detect single molecules [23]. In this field of application, a remarkable example is represented by both surface plasmon polaritons (SPPs) and surface enhanced Raman spectroscopy (SERS) where the Raman signal from the analysed molecules is enhanced by local plasmon resonances excited in proximity of metallic nano-particles [24, 25]. Even though these kinds of sensors present considerable resolution and sensitivity, the large optical absorption induced by metallic layer can produce a local heating and eventually damages in the biological material. For these reasons, the research and the development of alternative non-metallic enhancing substrates are particularly appealing.

Previous studies have shown that negative index photonic crystals (NIPhCs) can support surface waves with similar features of surface plasmons in metals. The existence of these plasmon-like evanescent states has been experimentally observed and the agreement between the simulation and the measured data confirmed the surface plasmon-like nature of the measured wave [26]–[28].

In particular, the presence of the surface states from the 2D NIPhC slab has been detected by means of an evanescent-coupling method with a high refractive index prism and using standard ellipsometric measurements of Ψ and Δ values. In this case, it has been shown that a drastic change in sing of refractive index practically acts as the change in dielectric constant in plasmonic structures. Indeed, some resonances appear in Ψ spectrum, corresponding to a 180°jump in phase Δ. Moreover, the shape of these resonances are asymmetric like in the plasmonic nanostructure described by the Fano resonance [29]. A good agreement between the Fano model fit and the experimental data confirms that pure dielectric metamaterials behave like plasmon-polaritons materials, also in complete absence of free carriers.

In our experiments, the 3D problem of a light beam incident on a NIPhC slab with a wavevector $\vec{k}$ out of the slab plane has been considered. The NIPhC slab is constituted by a 2D hexagonal lattice of air holes in silicon and it is realized on a Silicon-on- Insulator (SOI) wafer. In a SOI wafer, the 1.5 μm thick top layer of silicon is large enough to ensure an effective 2D system behaviour. Indeed, the effective index for the fundamental mode supported by a uniform slab waveguide of this thickness is $n_{\text{eff TE,TM}} = 3.45$ for $\lambda = 1.55$ μm and it is equivalent to the bulk silicon value for both TE and TM polarizations. If the hole radius r and lattice parameter a have ratio $r/a = 0.385$, the EquiFrequency Surface (EFS) for TM polarization (the electric field directed along the holes axis) of such PhC around the normalised frequency $\omega_{\text{n}} = 0.305$ collapses to the origin of the Brillouin zone (Figure 1). This behaviour is opposed to its usual behaviour in positive refracting media, where the EFSs expand with increasing frequency. Also, the EFS calculated for frequencies around n have quite circular shape, like an isotropic medium (Figure 1). The group velocity, $\vec{v}_g \equiv \partial\omega/\partial\vec{k}$, is inwardly directed, in opposite to the direction of the corresponding wavevector, so that $\vec{v}_g \cdot \vec{k} < 0$. Also, this PhC behaves as a medium with effective index $n_{\text{eff}} = 1$ for the normalised frequency $\omega_{\text{n}} = 0.305$. For $\lambda = 1.55$ μm, this corresponds to holes radius $r = 180$ nm and lattice period $a = 472$ nm. A SEM image of a sample of this negative refracting PhC (NIPhC) is shown in Figure 2.

Let $\vec{k} = \vec{k} + \vec{k}_{\parallel}$ the wavevector of a plane wave coming from air and incident on the PhC slab. Respect to the slab structure, $\vec{k}_{\parallel}$ and $\vec{k} \neq 0$ are the in-plane and the orthogonal components, respectively. The in-plane component $\vec{k}_{\parallel}$ is conserved at interfaces and is influenced by the periodic lattice of the PhC. For a plane wave with $\omega_{\text{n}} = 0.305$ at TM polarization, the match between the dispersion relations of the air and the NIPhC strongly favourites the coupling between the incident $\vec{k}$-vector and the wavevector propagating in the NIPhC (see dashed and red circles in Figure 1), resulting in a very low reflection. This behaviour is the same of that described by the

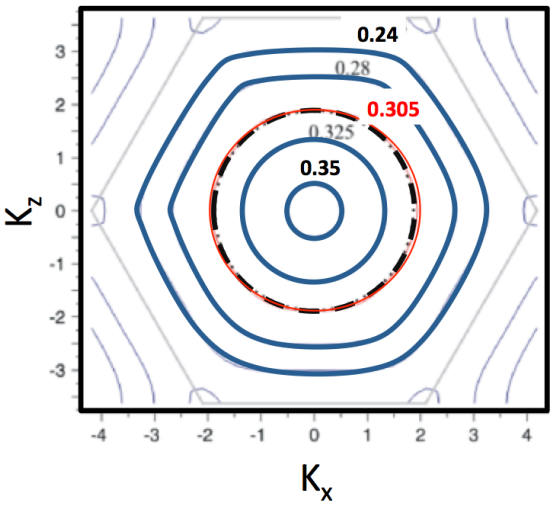

FIG. 1 The EquiFrequency Surfaces contours of a silicon (ϵ = 11.9) air-holes PhC with normalised radius r/a = 0.385, for TM polarization in the (k_z,k_x) plane, where (k_x,k_y,k_z) defines the reciprocal space of the PhC. The blue lines show the EFS contours at normalized frequencies ω = 0.24, 0.28, 0.325 and 0.35, respectively. The red line shows the EFS contour at ω_n = 0.305. The dashed circle is the air dispersion curve for ω_n = 0.305.

plasmonpolariton coupling between materials with opposite dielectric constant ϵ. In both cases a propagating wave in the direction parallel to the interface is excited and a resonance appears in the reflection spectrum.

In Figure 2, the experimental spectra of the reflectance in p polarization (corresponding to TE polarization in the slab plane) and s polarization (corresponding to TM polarization in the plane) for the NIPhC are presented and are called $R_{p\mathrm{PhC}}$ and $R_{s\mathrm{PhC}}$, respectively. It is evident a resonance around the wavelength $\lambda_0 = 1.55$ µm, where the refraction behaviour is negative.

A further analysis of resonances is obtained by means of the ellipsometric measurements as in [30], where a plasmonic resonance is recognized as a peak in Ψ spectrum and a 180°shift in Δ spectrum, where Ψ and Δ are the standard ellipsometric parameter defined by the equation:

$$\frac{r_p}{r_s} = \tan\Psi e^{-i\Delta} \tag{1}$$

where r_p and r_s are the Fresnel complex coefficients. In the ellipsometric experimental results for the NIPhC we clearly recognize a plasmon-like resonance at $\lambda_0 = 1.55$ µm (Figure 3(a). Peaks due to a simple guided mode are shown at wavelengths between 1420 nm and 1470 nm in Figure 3(a)). Otherwise, at wavelengths for which the refraction behaviour is negative, a jump of about 180°in Δ spectrum corresponds to the peak in Ψ spectrum. Also, unlike the peaks due to the guided modes in the periodic structure [21], by varying the incidence θ angle between the incidence plane and the Γ-K symmetry direction of the NIPhC (see Figure 3(c)), the resonance at $\lambda_0 = 1.55$ µm shows a isotropic property, due to the quite perfect circular shape of the EFS contour (Figure 1) at $\lambda_0 = 1.55$ µm.

Moreover, the $R_{s\mathrm{PhC}}$ measurements test the whole irreducible Brillouin zone in the $\vec{k}$ space, by rotating the sample between $\theta = -15°$ and +15° and at fixed $\phi = 70°$, for the hexagonal lattice symmetry invariances (Figure 3(b)). At $\lambda_0 = 1.55$ µm the

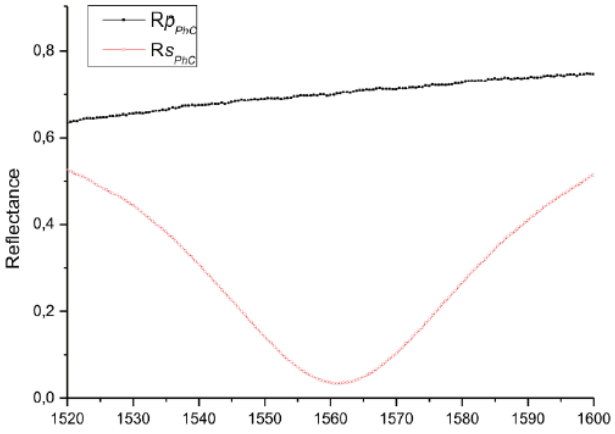

(a)

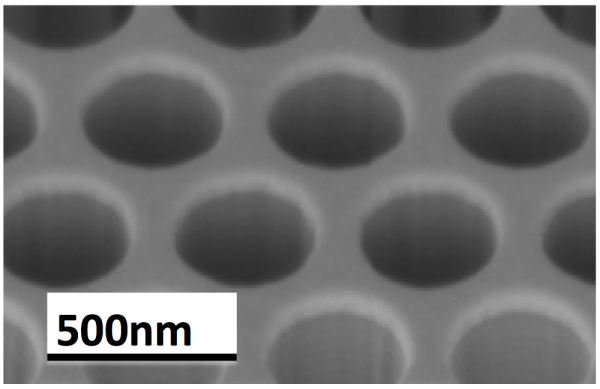

(b)

FIG. 2 (a) Normalized reflectance measurement: reflectance in p polarization (corresponding to TE polarization in the plane) and s polarization (corresponding to TM polarization in the plane) for the NIPhC are presented and are called $R_{p_{\mathrm{PhC}}}$ and $R_{s_{\mathrm{PhC}}}$, respectively. At λ = 1555 nm deep resonance appears in the $R_{s_{\mathrm{PhC}}}$ spectrum. (b) SEM image of the sample.

graph shows that the shape and the depth of the resonances are almost the same for all angles, confirming the ellipsometric measurements. Indeed, the same peak at $\lambda_0 = 1.55$ µm is well recognized as θ varying, whereas other resonances aren't simply transformed (Figure 3(b)). Thus, any incident $\vec{k}$-vector at $\lambda_0 = 1.55$ µm and TM polarization excites a propagative mode, which confines light parallel to the PhC slab, acting as polaritonic excitations in plasmonic structures, in spite of the absence of free carrier in the dielectric silicon based photonic structure.

A further analogy with plasmonic behaviour arises by the asymmetric shape of the experimental Ψ spectrum [29]. Indeed, using Fano resonance model for fitting experimental data a good agreement is achieve. In Figure 4 the Ψ spectrum are plotted with Fano model equation:

$$f(\omega) = A + F\frac{(q\gamma + \omega - \omega_0)^2}{(\omega - \omega_0)^2 + \gamma^2}, \tag{2}$$

where γ and ω_0 are the width and the frequency of the resonance, respectively, and q is the Fano factor which determines the asymmetrical shape.

Furthermore, in negative PhC slabs the presence of guided mode resonances (GMRs) have been demonstrated, where sharp resonances in the reflection and transmission spectra appear when incident radiation is coupled with the modes of

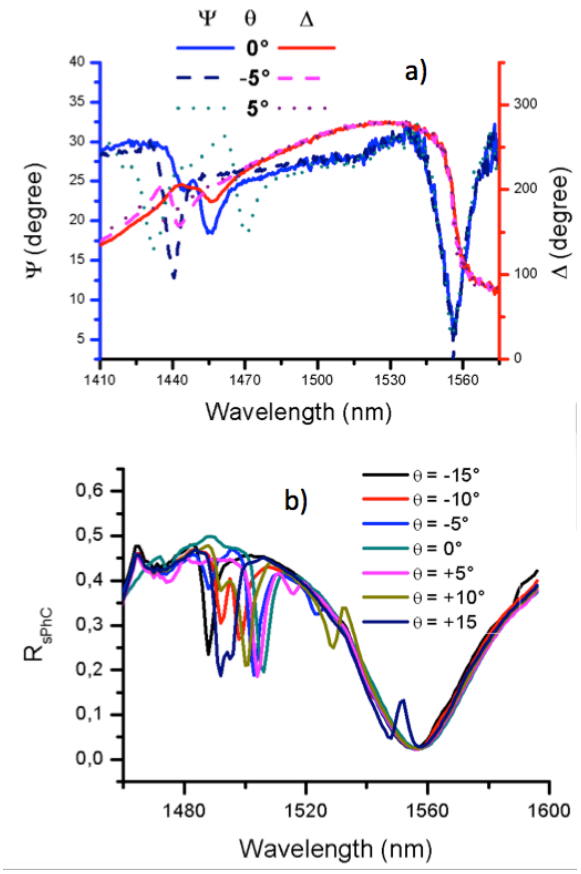

FIG. 3 (a) Ellipsometric results: lines in blue tones define Ψ spectra, lines in red tones define Δ spectra. At λ_0 = 1.55 μm, the peak in Ψ is almost unchanged and the 180°shift in Δ spectrum appears for all θ angles. (b) Reflectance spectrum R_{sPhC} for some θ angles in the irreducible Brillouin zone. By varying θ, the peak at λ_0 = 1.55 μm doesn't change shape and depth, whereas other peaks shift in wavelength and generally change shape. c) Geometry of measurements: θ is the incidence angle defined as the angle between the incidence plane (light blue plane) and the Γ-K symmetry direction (red arrow) of the hexagonal lattice.

the structure [31]. The reflection spectra are collected by varying the incident angle: when the coupling between the incident radiation and a guided mode occurs, a sharp peak appears in the collected signal.

Whenever coupling occurs, the radiation propagates for few millimeters into the photonic crystal. By using an IR-camera we collected the images of the radiation coupled into the structure under resonance condition. Interestingly, back propagation of the coupled radiation was observed, which can be related to the negative index behaviour of the photonic crystal under consideration (Figure 5).

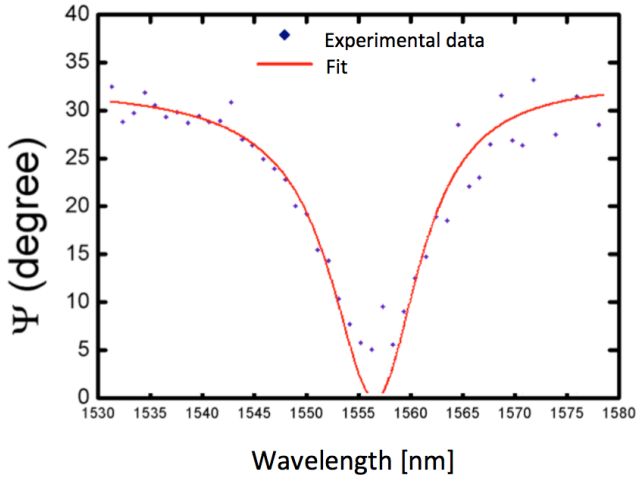

FIG. 4 Using Fano resonance model for fitting experimental Ψ data a good agreement is achieved.

Rigorous Coupled-Wave Approach (RCWA) simulations provided further information regarding this phenomenon. The calculated time-averaged Poynting vector inverts its direction while crossing the photonic crystal (Figure 6).

Finally, we use a new theoretical approach by directly fitting the experimental spectrum. In [27] we experimentally demonstrated that, in the range of negative effective refractive index, a photonic crystal can be modelled as a Lorentz resonator. In this way, the resonator behaviour is inherent into the material, and the PhC is described as an homogenous material with $\epsilon(\omega)$ given by:

$$\epsilon = \frac{f\omega_0^2}{\omega_0^2 - \omega^2 + i\gamma\omega} + \epsilon_\infty \qquad (3)$$

In such a case, we can use the usual Fresnel relations to study the features of guided resonances in the reflectivity spectrum, by considering the slab as a three-layer system air/PhC Lorentz/substrate. The calculated fit curve shows an excellent agreement with the experimental spectrum, as reported in Figure 7(a). In addition, by changing the incident angle, the band structure of the photonic crystal can be determined. Once again, the measured values (squares) are in excellent agreement with the simulated dispersion curve (triangles) obtained from the RCWA (Figure 7(b)).

Very recently it has been shown that a very high quality factor (Q) can be achieved in thin photonic crystal slab with high-index [32]. Typically these are Fano resonances that, under special condition, can have long lifetimes. In a special subset of design parameters, Q factor have been anticipated to approach infinity [33, 34]. We demonstrated that a suitable design of a thin photonic crystal membrane realized with silicon nitride can exhibit a 700-fold field enhancement, evaluated respect to the amplitude of the incident field (Figure 8). The evolution of such Fano resonances toward a true bound state within the radiation continuum, formally similar to quantum systems with bound states above the continuum threshold [35], is the origin of this phenomenon. All these resonant

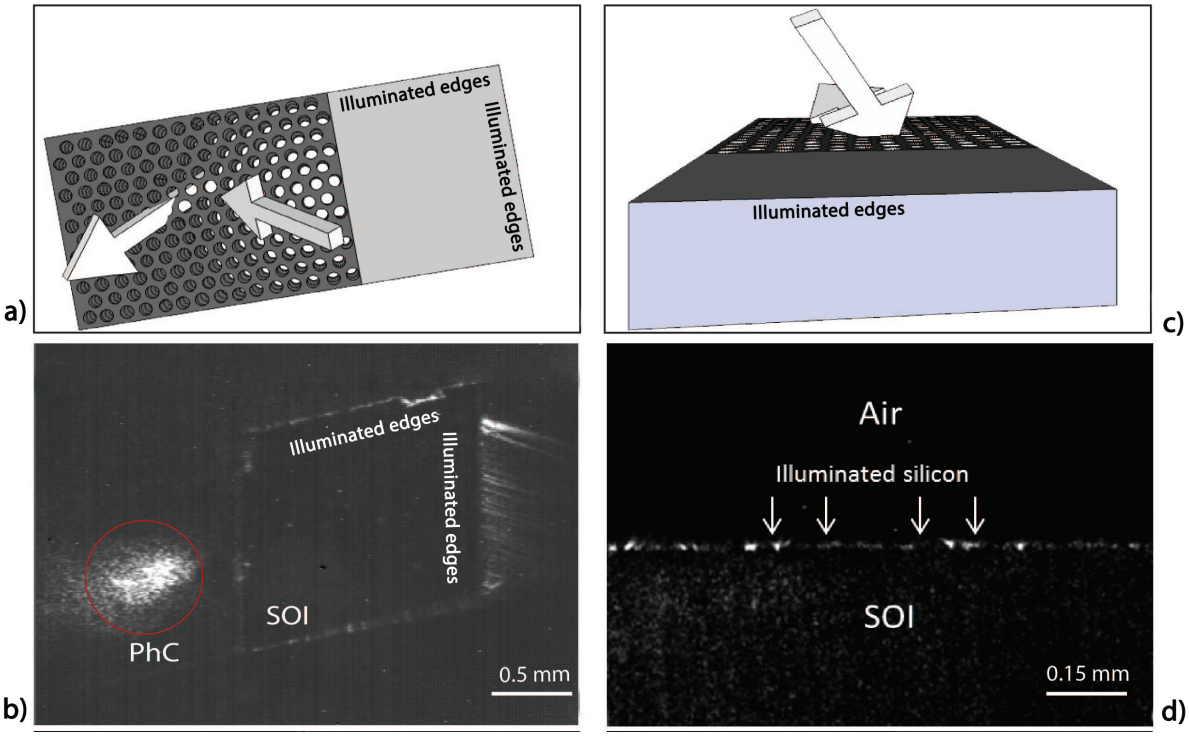

FIG. 5 Sketches of the IR camera positions (a, c) and infrared images of the illuminated SOI region when resonance occurs (b, d). The red circle indicates the spot at which the laser is incident on the sample. Abbreviations: IR, infrared; SOI, silicon-on-insulator; PhC, photonic crystal.

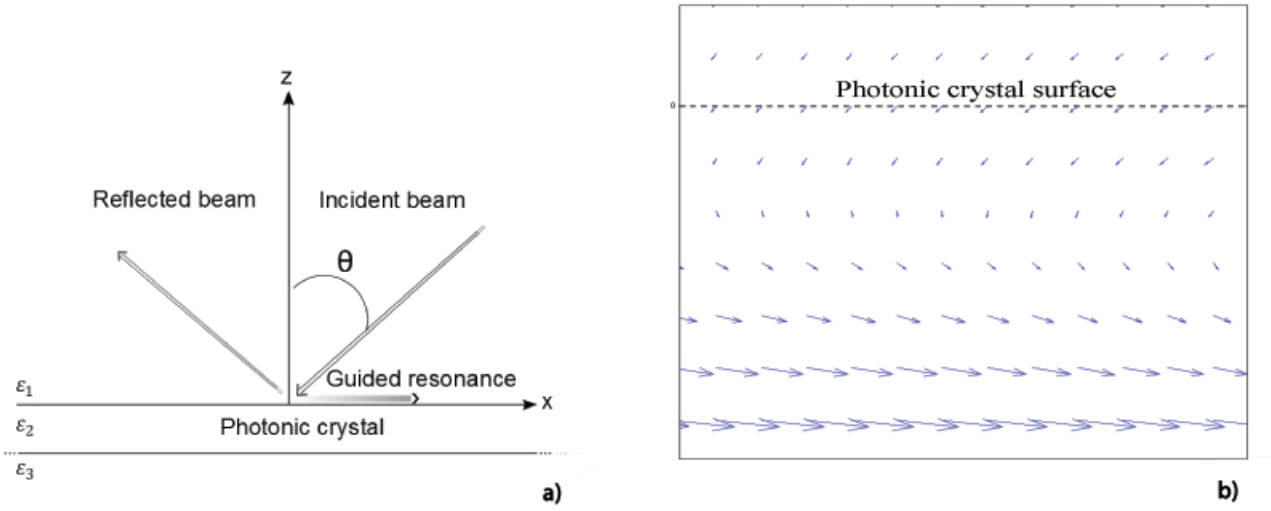

FIG. 6 (a) A sketch of the incident, reflected and guided beams. (b) The calculated time-averaged Poynting vector in a 60×60 nm² area in the *xz*-plane, crossing the PhC surface under the resonance conditions. PhC, photonic crystal.

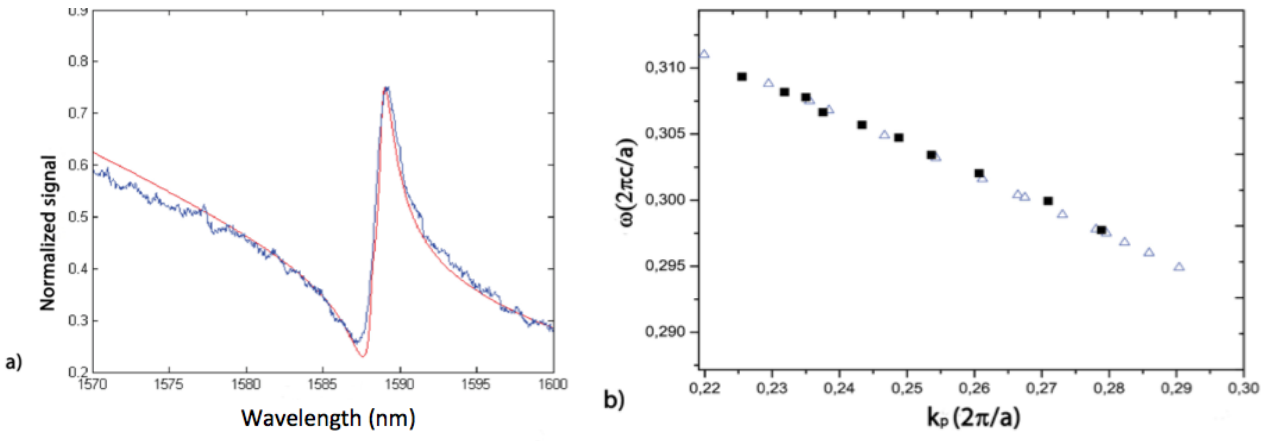

FIG. 7 a) Comparison between theoretical and experimental values. The fitted curve (red line) shows good agreement with the experimental spectrum (blue line). b) Comparison between the calculated (triangles) and measured (squares) band structures.

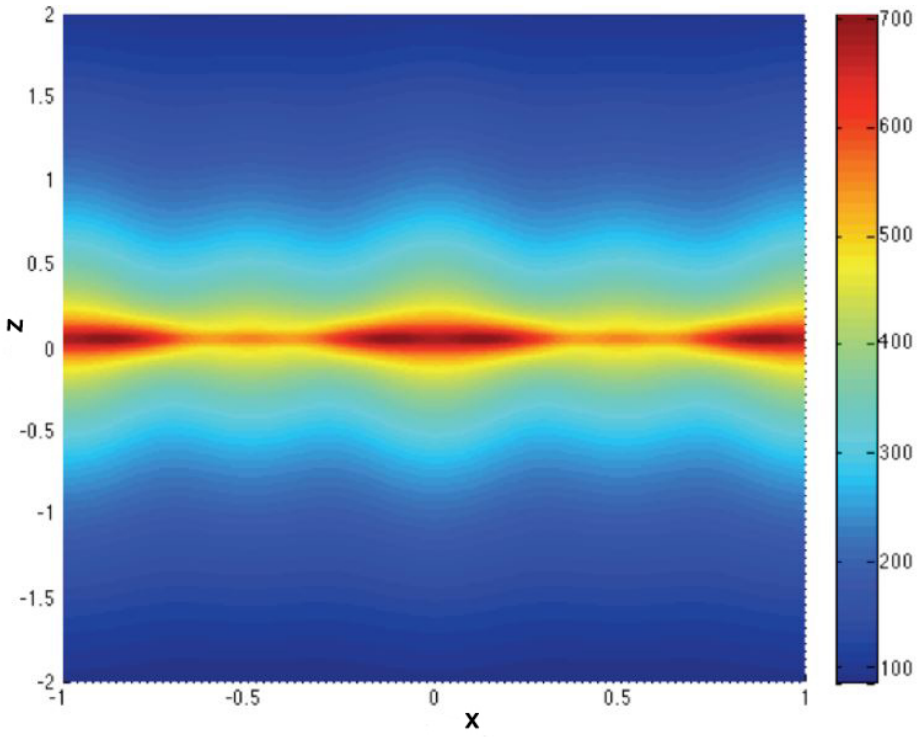

FIG. 8 A vertical cut of the Electric Field amplitude in resonance condition calculated by using FTDT approach in the unit cell.

states may have a variety of potential applications because it involves very narrow coupled resonances with a high Q value in an open structure and in lossfree media.

3 NEAR INFRARED SILICON PHOTODETECTORS

In order to develop all-Si PD and to take advantage of low-cost standard Si-CMOS processing technology without additional material or process steps, a number of options have been proposed: two-photons absorption (TPA) [36], incorporation of optical dopants/defects with midbandgap energy levels into the Si lattice [37] and internal photoemission effect (IPE) [38]. The main advantages of these devices reside in their extremely large bandwidth and simple fabrication process, but, unfortunately, their efficiency is very low.

IPE is the optical excitation of electrons in the metal to energy above the Schottky barrier and then transport of these electrons to the conduction band of the semiconductor. The standard IPE theory is due to Fowler [39]. However, the Fowler's theory was obtained without taking into account the thickness of the Schottky metal layer. The enhancement of IPE in thin metal film was theoretically investigated by Vicker who introduce a multiplicative factor to the Fowler's formula [40]. Finally, a further enhancement in IPE can be obtained due to the increase of the reverse voltage which lower the Schottky barrier increasing the amount of emitted carriers [38]. Concerning photodetectors, due to the very low signal-to-noise ratio, for a long time IPE-based Si PDs, at IR wavelengths, were believed usable only at cryogenic temperature. However, in order to enhance the photoemitted current with respect to the noise dark current, many structures have been proposed based on: surface plasmon polaritons (SPP) [41], micro- and nano-metric optical waveguide [42], optical microcavity [43].

3.1 IPE enhancement by an optical microcavity

In 2008, we experimentally demonstrated the influence of the optical microcavity on IPE for a Schottky Si junction [43]. In that work we proposed a device realized by a resonant cavity Fabry-Perot structure formed by a dielectric bottom mirror, a metallic top mirror and, in the middle, a silicon cavity (Figure 9(a)). The dielectric bottom mirror is a distributed Bragg reflector (DBR) formed by alternating layers of amorphous hydrogenated silicon (a-Si:H) and silicon nitride (Si_3N_4) having $\lambda/4$ thicknesses, while, the top mirror was realized by a copper (Cu) layer working both as absorbing material and as optical mirror.

Responsivity measurements were carried out in the range of 1545–1558 nm (step of 0.05 nm) showing a cavity finesse F and responsivity of 4.7 and 4.3 μA/W, respectively, for a DBR realised with five pairs of Si_3N_4/a-Si:H (reflectivity 99%). Then, in the 2010 we showed that by reducing the size of the device a further increase in responsivity of twice (its value was about 8 μA) could be obtained [44]. Finally, in 2012 we demonstrated, both theoretically and experimentally, that a significant increase in responsivity of 0.063 mA/W could be obtained by fulfilling the critical coupling conditions (Figure 9(b)) [45].

3.2 IPE enhancement by a waveguide structure

From the IPE theory is well-known that emission of photogenerated carriers into silicon can be increased by lowering the potential barrier. It can be obtained by applying a reverse bias to the Schottky junction [38], but, unfortunately, the higher the revere voltage, the higher the dark current. Increase in dark current could be limited by re-

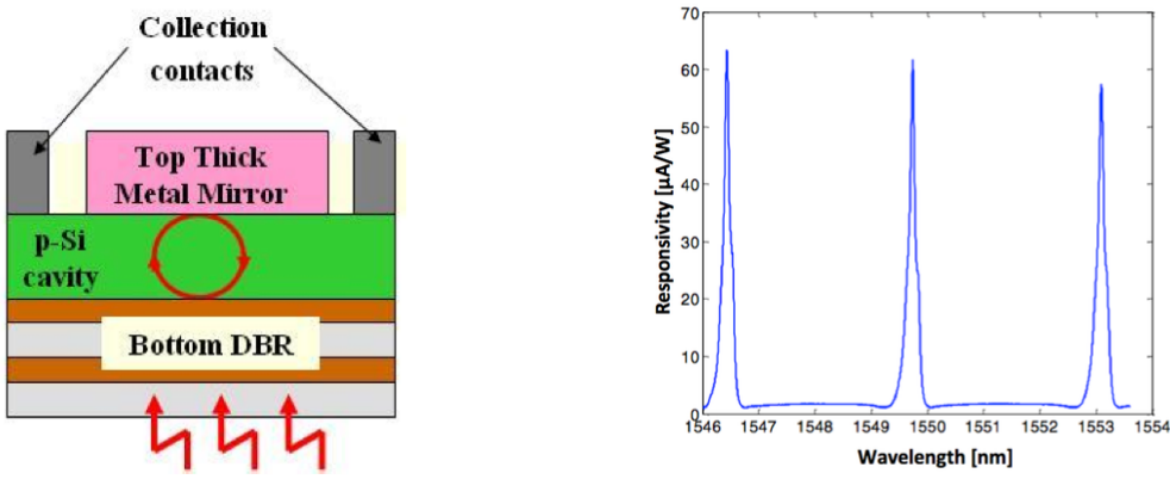

(a) (b)

FIG. 9 PD reported in ref. [43]-[45]: (a) Schematic cross section and (b) responsivity vs wavelength [45].

ducing the Cu active area in contact with Si but, in this case, the light coupling on a small size of absorbing layer is not a trivial task to reach. A guiding structure can be used in order to overcome this drawback. Very recently we proposed a silicon-oninsulator (SOI) waveguide asymmetric metal-semiconductor-metal (MSM) PD based on IPE and working at 1550 nm (Figure 10(a)) [46]. The main novelty of the structure was that the absorbing metal (Cu) is in contact with silicon only on the vertical wall of the optical waveguide. The main advantage was that the device is able to tackle typical responsivity/dark current trade-off, afflicting IPE-based devices performances. Taking advantage of a small contact area of about 3 μm^2 it was possible to increase the reverse applied voltage up to 21 V with a very low dark current of 2.2 nA. In addition an increased responsivity of 4.5 mA/W (Figure 10(b)), and a bandwidth of 1 GHz were demonstrated. Finally, the device exhibits the capability to extend its wavelength cut-off under an applied reverse bias and could be useful for applications in the mid-infrared regime [46].

Unfortunately, device responsivity is greatly afflicted by losses due to reflections of the travelling radiation on the Cu metal layer; hence only a small amount of light can be effectively absorbed. This drawback could be overcome by creating an optical microcavity fabricated by etching deep trenches on the silicon rib waveguide in order to realize a grating reflector. Grating design is very important to fulfil critical coupling conditions. Starting from a SOI substrate (3-μm-thick buried oxide and 1.5-μm-thick top Si), a 2-μm-width rib waveguide has been designed to have mono-modal behaviour (rib height: 1.5 μm and slab height: 1.05 μm) and the results of our simulations of Figure 11(a) show a fundamental mode effective refractive index of 3.456. In addition, we have calculated than the effective refractive indices span between 3.424 and 3.456 when the rib height are 1.05 μm and 1.5 μm, respectively (Figure 11(b)).

By considering 3.424 as low refractive index and 3.456 as high refractive index and taking into account the Bragg wavelength (λ_B):

$$\lambda_B = 2n_{eff}\Lambda, \tag{4}$$

where n_{eff} and Λ are the effective refractive index and the grating period, respectively, a grating period of about 224 nm and a grating length of 56 μm at 1550 nm can be estimated to fulfil critical coupling conditions.

3.3 IPE enhancement by two-dimensional materials (graphene)

In a recent paper Amirmazlaghani et al. [47] show that canonical Fowler's theory is not suitable to describe Schottky junctions where a two-dimensional layer plays the role of the metal. The main reason is that, due to the two dimensionality of the material, the photoexcited carriers have more chance to gain the right momentum to overcome the Schottky barrier providing a significantly increase in responsivity. Graphene is a twodimensional emerging material that is able to form a Schottky junction on Si [48] and due to its excellent electrical properties it is the best option to realize IPE-based devices. Responsivity (R) of IPE-based graphene/Si Schottky PD can be calculated as [47]:

$$R = \frac{\lambda}{1.24} \cdot \frac{A}{2} \cdot \frac{\left(\frac{1.24}{\lambda}\right)^2 - \Phi_B^2}{\left(\frac{1.24}{\lambda}\right)^2} \tag{5}$$

where λ is the wavelength, A the graphene absorption and Φ_B is the graphene/Si Schottky barrier.Unfortunately due to the low graphene absorption (only 2.3%) only a limited responsivity can be expected, however, by introducing the Schottky junction inside e Fabry-Perot microcavity a significant increase in responsivity can be obtained. In the following, the design of a microcavity Schottky graphene/Si PD, based on internal photoemission effect at 1.55 μm and working at room temperature, is described and its efficiency has been numerically calculated. Proposed device is similar to that shown in Figure 9(a) where metal is replaced by a graphene layer. It is a very simple Fabry-Perot vertical-to-the-surface structure formed by a bottom and a top metal mirror surrounding a $\lambda/2$ silicon layer. While the graphene/silicon interfaces acts as top mirror, a distributed Bragg reflector (DBR) serves as bottom mirror. DBR could be realized by alternating layers of amorphous hydrogenated silicon (a-Si:H) and silicon nitride (Si_3N_4) deposited by a plasma enhanced chemical vapour deposition (PECVD) technique as we have shown in our pre-

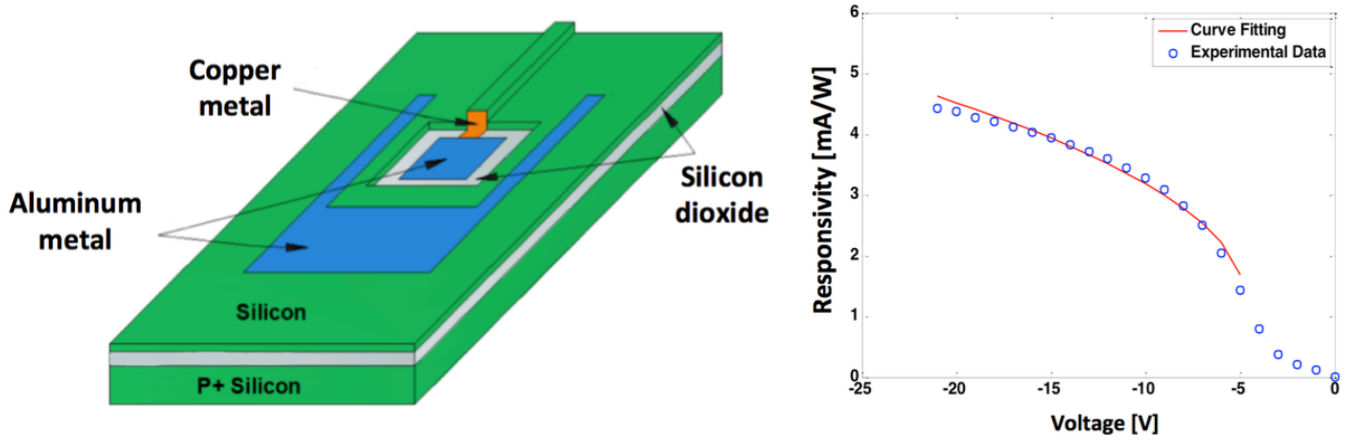

(a) (b)

FIG. 10 PD proposed in ref. [46]: (a) sketch, (b) responsivity vs reverse voltage.

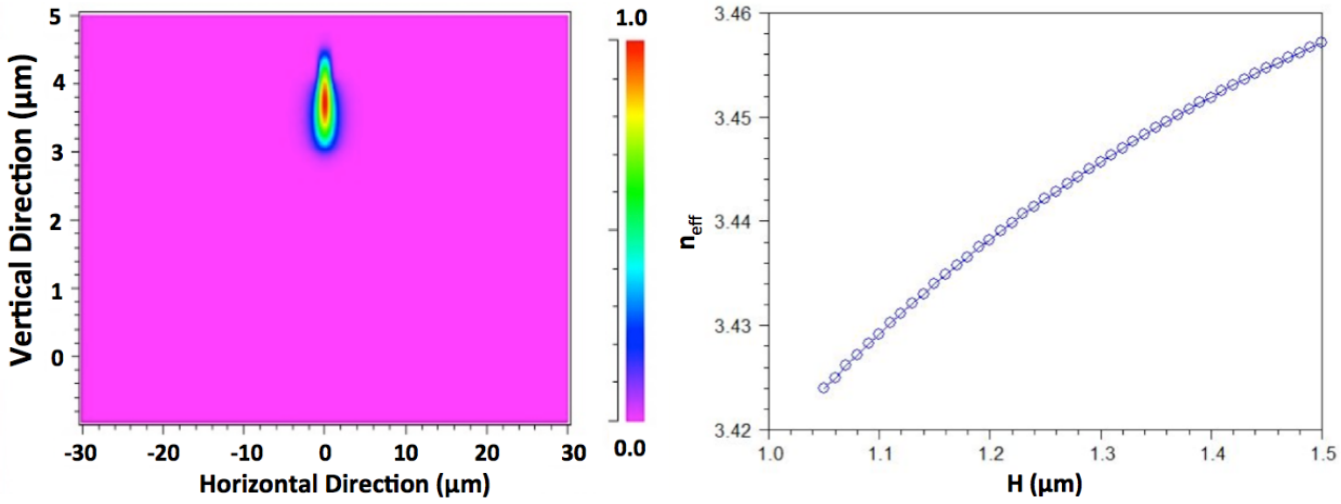

(a) (b)

FIG. 11 (a) Simulated transverse mode profile for a SOI waveguide with a rib height of 1.5 µm and a slab height of 1.05 µm. (b) Simulated change in refractive index in function of the rib height (H) while slab height is considered fixed at 1.05 µm.

vious work. The samples could be fabricated starting from a quasiintrinsic bi-polished 100-µm-thick silicon wafer. Substrate should be chosen quasiintrinsic in order to avoid free carrier absorption.

In order to estimate the theoretical quantum efficiency of the graphene/Si PD, we take advantage of Eq. (5) while for the absorption calculation a numerical method, based on the Transfer Matrix Method [49], has been used. By taking into account the refractive indices at 1550 nm of graphene ($3+i1.81\lambda$) [50], Si (3.45) [51], Si_3N_4 (1.82) [44] a-Si:H (3.58) [44] and a potential barrier Φ_B of 0.76 eV [52], Figure 12 can be derived.

Figure 12 shows the effects of the cavity on the device performance. It is worth noting that the higher the DBR reflectivity, the higher the device responsiviy. We note that a maximum responsivity enhancement of more than two order of magnitude, due to the presence of a 5-pair DBR, can be achieved with respect to the structure where no cavity effects are considered. Device with no DBR has been fabricated in our cleanroom and its responsivity is higher more than one order of magnitude than that of a similar device realized with Cu [43]. Graphene/Si Schottky PDs incorporated into a microcavity structure are very promising to be employed in the telecommunications.

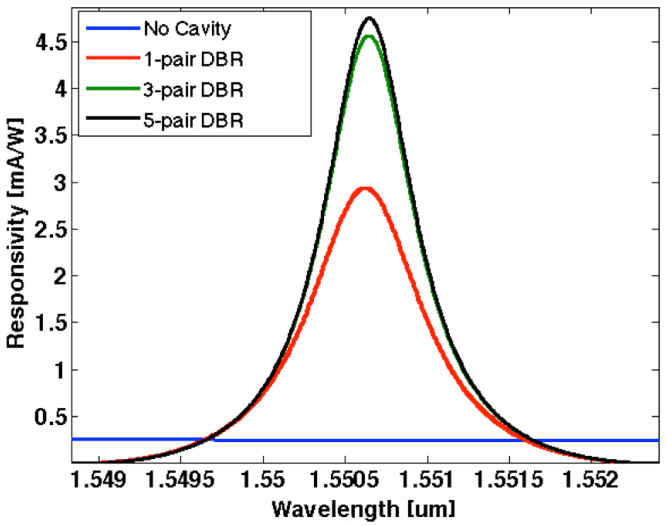

FIG. 12 Calculated responsivity vs wavelength for the graphene/Si PD provided of 1-pair (red line), 3-pair(green line) and 5-pair (black line) a-Si:H/Si_3N_4 DBR, while blue line refers to a PD device with no effect.

4 SILICON BASED MICROARRAY FOR BIOMEDICAL APPLICATIONS

Silicon, and silicon related materials, has been by far largely exploited in the field of biomedical applications due the standard high precision fabrication techniques. Siliconbased optical microarrays are among the most used devices [53]: even if in genomic experiments this technology has been replaced by deep sequencing, microarray is still a workhorse in small laboratories everyday work, especially in proteomic and personalized medicine. The fabrication of such a device requires the selection of a proper mask material that should protect the silicon surface during the integration of a transducer element: for example, is this the case of electrochemical etching process needed for the realization of porous silicon (PSi) optical elements. The standard material used is chemical vapour deposited silicon nitride, which is a very effective masking material against electrochemical dissolution, but often does not allow thermal oxidation due to surface cracking in case of hydrogen escape at high temperatures. As some alternative approaches, we exploited the plasma deposited amorphous silicon and the SU8 photoresist as masking materials [54, 55]. In the following, we report our best achievements in microarrays fabrication by using these two alternative approaches, in comparison to the standard silicon nitride process. The device designed is a photonic microarray of porous silicon Bragg reflectors on a crystalline silicon substrate that has been realized using a technological process based on standard photolithographyand electrochemical anodization of the silicon. The array density is of 170 elements/cm^2 and each element has a diameter of 200 μm. All fabrication steps have been monitored by spectroscopic optical reflectometry. The integration of porous silicon elements in a microarray, a proper technological process had to be designed, depending on the masking material used. The silicon substrate was a highly doped p$^+$-type wafer with a resistivity of 0.001 Ωcm, $<100>$ oriented and 500 μm tick. The first microarray has been fabricated by using amorphous silicon as masking material. The photoresist ARN4340 was spin coated on the silicon substrate and patterned by a standard photolithographic process, in order to obtain silicon spots of 200 μm. Then, a 600 nm thick layer of amorphous silicon has been deposited on the substrate by sputtering process; the substrate was washed in piranha 100°C for 20 min, in order to remove photoresist. Finally, the silicon wafer with amorphous silicon mask was electrochemically anodized in a HF-based solution (50 wt. % HF : ethanol = 1:1) in dark and at room temperature. The result of the electrochemical etching is shown in Figure 13 that shows uniform PSi regions (in green).

The reflectivity spectra of the Bragg mirrors at normal incidence, randomly chosen in the whole area, are characterized by resonance peaks around 1032 nm and a FWHM of about 57 nm (Figure 14). The proximity of all peaks in the spectra is an indirect proof of the electrochemical etch homogeneity on the whole microarray surface.

The second microarray fabrication flow process is based on a direct use of the SU8 photoresist as masking material: in particular, a layer of about 10 μm thick was spincoated on the substrate and patterned by a standard photolithographic process in order to obtain free silicon spots of 200 μm. Finally, the silicon wafer was electrochemically anodized as previously described. The result of the electrochemical etching is shown in Figure 15.

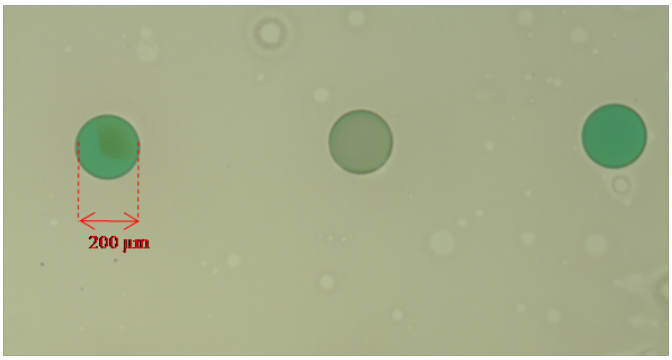

FIG. 13 Porous silicon elements realized by masking the silicon with amorphous silicon.

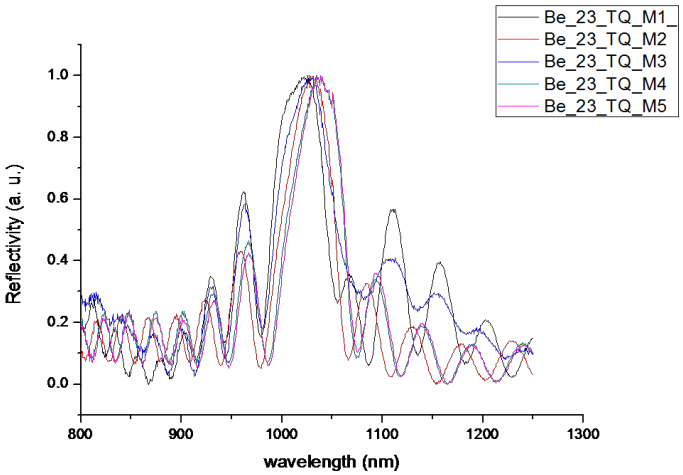

FIG. 14 Reflectivity spectra of the PSi Bragg mirrors.

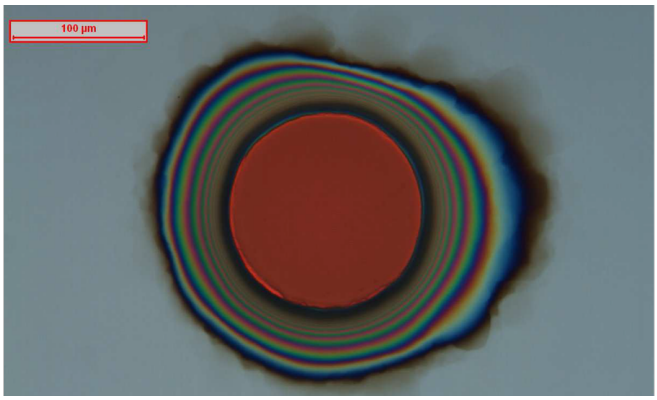

FIG. 15 A porous silicon element realized masking the silicon with SU8 photoresist.

The silicon nitride based technology requires a more complex process flow, in particular the deposition of a 1.6 μm thick layer by PECVD. A standard photolithographic process was used to pattern the silicon nitride film, which has been subsequently etched by RIE process in CHF_3/O_2 atmosphere. Finally, the silicon wafer was electrochemically anodized as previously described. The process is not as simple as those aforementioned, and more than one technological step is required. However, the results are better than those with photoresist, from both mechanical and optical point of views. The optical microscope image of the microarray and the reflectivity spectra of some Bragg mirror elements are reported in Figure 16.

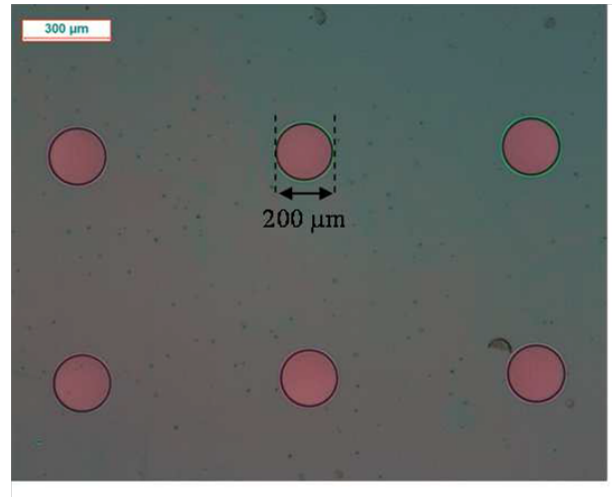

(a)

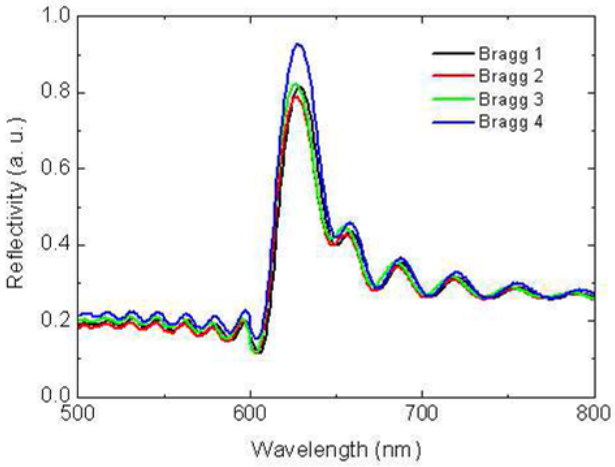

(b)

FIG. 16 Optical microscope image of the microarray and reflectivity spectra of the PSi Bragg mirrors obtained by using silicon nitride film.

In this case, there is not any under-etching below the mask material and the optical spectra of different photonic element are really very similar, thus confirming the uniformity of the PSi fabrication on the whole area.

These structures can be easily integrated with microfluidic circuits constituting low-cost, easy to use lab-on-chip for biomedical applications [55, 56].

5 CONCLUSIONS

In this work we have reported on the advances of our activity in the field of Si micro and nanophotonics. First, we have reported on Fano resonances in dielectric negative refracting PhC and we have showed that a design of a thin slab negative refracting PhC realized with silicon nitride can exhibit a 700-fold field enhancement (evaluated respect to the amplitude of the incident field) resulting very promising for all photonic silicon devices based on nonlinear phenomena. Concerning photodetection, PDs based on IPE working at 1550 nm and at room temperature, have been reported. The best performance of our device in term of responsivity, bandwidth and dark current are 4.5 mA/W, 1 GHz and 2.2 nA, respectively. Our results demonstrate that these devices are already suitable for power monitoring applications and new perspectives seem to be opened by the rise of new two dimensional material like graphene. Finally a microarray of porous silicon Bragg reflectors, on a crystalline silicon substrate, have been realized using a technological process based on standard photolithography and electrochemical anodization of the silicon. The array density is of 170 elements/cm^2 and each element has a diameter of 200 µm. All fabrication steps have been monitored by spectroscopic optical reflectometry. To integrate porous silicon elements in a microarray, a proper technological process has been designed. We believe that our results will be able to open new frontiers in the field of low-cost silicon micro and nanophotonics.

6 ACKNOWLEDGEMENTS

Authors sincerely thank Dr. Mario Iodice, Dr. Mariano Gioffrè and Dr. Luigi Sirleto for fruitful discussions and feedback on the contents of this work.

References

[1] B. Jalali, "Silicon photonics," J. Lightw. Technol. **24**, 4600–4615 (2006).

[2] R. A. Soref, "The past, present, and future of silicon photonics," J. Sel. Top. Quantum Electron. **12**, 678–1687 (2006).

[3] R. A. Soref, and J. Lorenzo, "All-silicon active and passive guided-wave components for λ = 1.3 and 1.6 µm," IEEE J. Quantum Electron. **22**, 873–879 (1986).

[4] R. A. Soref, and B. R. Bennett, "Kramers-Kronig analysis of E-O switching in silicon," Proc. SPIE Integr. Opt. Circuit Eng. **704**, 32–37 (1986).

[5] B. Schuppert, J. Schmidtchen, and K. Petermann, "Optical channel waveguides in silicon diffused from GeSi alloy," Electron. Lett. **25**, 1500–1502 (1989).

[6] R. A. Soref, J. Schmidtchen, and K. Petermann, "Large single-mode rib waveguides in GeSi and Si-on-SiO_2," IEEE J. Quantum Electron. **27**, 1971–1974 (1991).

[7] L. K. Rowe, M. Elsey, N. G. Tarr, A. P. Knights, and E, Post, "CMOS-compatible optical rib waveguides defined by local oxidation of silicon," Electron. Lett. **43**, 392–393 (2007).

[8] L. Vivien, D. Pascal, S. Lardenois, D. Marris-Morini, E. Cassan, F. Grillot, S. Laval, et al., "Light injection in SOI microwaveguides using high-efficiency grating couplers," J. Lightw. Technol. **24**, 3810–3815 (2006).

[9] Q. Xu, S. Manipatruni, B. Schmidt, J. Shakya, and M. Lipson, "12.5 Gbit/s carrierinjection- based silicon micro-ring silicon modulators," Opt. Express **15**, 430–436 (2007).

[10] C. P. Michael, M. Borselli, T. J. Johnson, C. Chrystal, and O. Painter, "An optical fiber-taper probe for wafer-scale microphotonic device characterization," Opt. Express **15**, 4745–4752 (2007).

[11] A. Liu, L. Liao, D. Rubin, H. Nguyen, B. Ciftcioglu, Y. Chetrit, N. Izhaky, et al., "High-speed optical modulation based on carrier depletion in a silicon waveguide," Opt. Express **15**, 660–668 (2007).

[12] A. Liu, R. Jones, O. Cohen, D. Hak, and M. Paniccia, "Optical amplification and lasing by stimulated Raman scattering in silicon waveguides," J. Lightw. Technol. **24**, 1440–1445 (2006).

[13] M. Casalino, L. Sirleto, L. Moretti, M. Gioffr; G. Coppola, M. Iodice, and I. Rendina, "Back-illuminated silicon resonant cavity enhanced photodetector at 1550 nm," Physica E **41**, 1097–1101 (2009).

[14] S. Rao, G. Coppola, M. A. Gioffrè, and F. G. Della Corte, "Hydrogenated amorphous silicon multi-SOI waveguide modulator with low voltage–length product," Opt. Laser Technol. **45**, 204–208 (2013).

[15] F. G. Della Corte, and S. Rao, "Use of amorphous silicon for active photonic devices," IEEE Transactions on Electron Devices **60**, 1495–1505 (2013).

[16] J. D. Joannopulos, R. D. Mead, and J. N. Winn, *Photonic crystals: molding the flow of light* (Princeton University Press, Princeton, 1995).

[17] S. G. Johnson, and J. D. Joannopoulos, *Photonic crystals: the road from theory to practice* (Kluwer Academic Publishers, New York, 2003).

[18] P. Dardano, L. Moretti, V. Mocella, L. Sirleto, and I. Rendina, "Investigation of a tunable T-shaped waveguides based on a silicon 2D photonic crystal," J. Opt. A-Pure Appl. Opt. **8**, S554–S560 (2006).

[19] M. Notomi, "Theory of light propagation in strongly modulated photonic crystals: Refractionlike behavior in the vicinity of the photonic band gap," Phys. Rev. B **62**, 10696–10705 (2000).

[20] V. Mocella, S. Cabrini, A. Chang, P. Dardano, L. Moretti, I. Rendina, D. Olynick, et al., "Self-collimation of light over millimeter-scale distance in a quasi-zero-average-index metamaterial," Phys. Rev. Lett. **102**, 133902 (2009).

[21] V. N. Astratov, D. M. Whittaker, I. S. Culshaw, R. M. Stevenson, M. S. Skolnick, T. F. Krauss, and R. De La Rue, "Photonic band-structure effects in the reflectivity of periodically patterned waveguides," Phys. Rev. B **60**, R16255 (1999).

[22] D. Peyradea, J. Torresa, D. Coquillata, R. Legrosa, J.P. Lascaraya, Y. Chenb, L. Manin-Ferlazzob, et al., "Equifrequency surfaces in GaN/sapphire photonic crystals," Physica E **17**, 423–425 (2003).

[23] X. Guo, "Surface plasmon resonance based biosensor technique: a review," J. Biophoton. **5**, 483–501 (2012).

[24] A. Giorgini, S. Avino, P. Malara, G. Gagliardi, M. Casalino, G. Coppola, M. Iodice, et al., "Surface-plasmon-resonance optical-cavity enhanced refractive index," Opt. Lett. **38**, 1951–1953 (2013).

[25] J. Kneipp, H. Kneipp, and K. Kneipp, "SERS- a single-molecule and nanoscale tool for bioanalytics," Chem. Rev. Soc. **37**, 1052–1060 (2008).

[26] E. De Tommasi, A. C. De Luca, S. Cabrini, I. Rendina, S. Romano, and V. Mocella, "Plasmon-like surface states in negative refractive index photonic crystals," Appl. Phys. Lett. **102**, 081113 (2013).

[27] P. Dardano, M. Gagliardi, I. Rendina, S. Cabrini, and V. mocella, "Ellipsometric determination of permittivity in a negative index photonic crystal metamaterial," Light Sci. Appl. **1**, e42 (2012).

[28] K. Ishizaki, and S. Noda, "Manipulation of photons at the surface of threedimensional photonic crystals," Nature **460**, 367–370 (2009).

[29] B. Luk'yanchunk, N. I. Zheludev, S. A. Maier, N. J. Halas, P. Ordlander, H. Giessen, and C. T. Chong, "The Fano resonance in plasmonic nanostructures and metamaterials," Nat. Mater. **9**, 707-715 (2010).

[30] V. G. Kravets, F. Schedin, and A. N. Grigorenko, "Extremely narrow plasmon resonances based on diffraction coupling of localized plasmons in arrays of metallic nanoparticles," Phys. Rev. Lett. **101**, 0087403 (2008).

[31] S. Romano, and V. Mocella, "Guided resonance in negative index photonic crystals: a new approach," Light Sci. Appl. **3**, 1–6 (2014).

[32] J. Lee, B. Zhen, S.-L. Chua, W. Qiu, J. D. Joannopoulos, M. Soljačić, and O. Shapira, "Observation and differentiation of unique high-Q optical resonances near zero wave Vector in macroscopic photonic crystal slabs," Phys. Rev. Lett. **109**, 067401 (2012).

[33] C. W. Hsu, B. Zhen, S. L. Chua, and S. G. Johnson, "Bloch surface eigenstates within the radiation continuum," Light Sci. Appl. **2**, e84 (2013).

[34] C. W. Hsu, B. Zhen, J. Lee, S.-L. Chua, S. G. Johnson, J. D. Joannopoulos, and M. Soljačić, "Observation of trapped light within the radiation continuum," Nature **499**, 188–191 (2013).

[35] J. Von Neumann, and E. Wigner, "Über merkwürdige diskrete Eigenwerte," Phys. Z **30**, 465–467 (1929) in German.

[36] T. Tanabe, H. Sumikura, H. Taniyama, A. Shinya, and M. Notomi, "All-silicon sub- Gb/s telecom detector with low dark current and high quantum efficiency on chip," Appl. Lett. **96**, 101103 (2010).

[37] D. F. Logan, P. Velha, M. Sorel, R. M. De La Rue, A. P. Knights, and P. E. Jessop, "Defect-enhanced silicon-on-insulator waveguide resonant photodetector with high sensitivity at 1.55 μm," IEEE Photonic. Tech. L. **22**, 1530-1532 (2010).

[38] M. Casalino, G. Coppola, M. Iodice, I. Rendina, and L. Sirleto, "Near-infrared sub-nandgap all-silicon photodetectors: state of the art and perspectives," Sensors **10**, 10571–10600 (2010).

[39] R. H. Fowler, "The analysis of photoelectric sensitivity curves for clean metals at various temperatures," Phys. Rev. **38**, 45–56 (1931).

[40] V. E. Vickers, "Model of schottky barrier hot-electron-mode photodetection," Appl. Opt. **10**, 2190–2192 (1971).

[41] P. Berini, A. Olivieri, and C. Chen, "Thin Au surface plasmon waveguide Schottky detectors on p-Si," Nanotechnology **23**, 444011 (2012).

[42] I. Goykhman, B. Desiatov, J. Khurgin, J. Shappir, and U. Levy, "Waveguide based compact silicon Schottky photodetector with enhanced responsivity in the telecom spectral band," Opt. Express **20**, 28594–28602 (2012).

[43] M. Casalino, L. Sirleto, L Moretti, M. Gioffrè, G. Coppola, and I. Rendina, "Silicon resonant cavity enhanced photodetector based on the internal photoemission effect at 1.55 micron: fabrication and characterization," Appl. Phys. Lett. **92**, 251104 (2008).

[44] M. Casalino, G. Coppola, M. Gioffrè, M. Iodice, L. Moretti, I. Rendina, and L. Sirelto, "Cavity enhanced internal photoemission effect in silicon photodiode for sub-bandgap detection," J. Lightwave Technol. **28**, 3266–3272 (2010).

[45] M. Casalino, G. Coppola, M. Iodice, I. Rendina, and L. Sirleto, "Critically coupled silicon Fabry-Perot photodetectors based on the internal photoemission effect at 1550 nm," Opt. Express **20**, 12599–12609 (2012).

[46] M. Casalino, M. Iodice, L. Sirleto, I. Rendina, and G. Coppola, "Asymmetric MSM sub-bandgap all-silicon photodetector with low dark current," Opt. Express **21**, 28072–28082 (2013).

[47] M. Amirmazlaghani, F. Raissi, O. Habibpour, J.Vukusic, and J. Stake, "Graphene-Si Schottky IR detector," IEEE J. Quant. Elect. **49**, 589–594 (2013).

[48] C. Chen, M. Aykol, C. Chang, A. F. J. Levi, and S. B. Cronin, "Graphene-silicon Schottky diodes," Nano Lett. **11**, 1863–1867 (2011).

[49] M. A. Muriel, and A. Carballar, "Internal field distributions in fiber Bragg gratings," IEEE Photonic. Tech. L. **9**, 955–957 (1997).

[50] M. Furchi, A. Urich, A. Pospischil, G. Lilley, K. Unterrainer, H. Detz, P. Klang, et al., "Microcavity-integrated graphene photodetector," Nano Lett. **13**, 2773–2777 (2012).

[51] E. D. Palik, *Handbook of optical constants of solids* (Academic Press, San Diego, 1998).

[52] M. Casalino, G. Coppola, M. Iodice, I. Rendina, U. Sassi, A. Lombardo, S. Milana, et al., "Silicon photodetectors based on internal photoemission effect: the challenge of detecting near infrared light," in *Proceedings to the 16th International Conference on Transparent Optical Networks*, 1–4 (IEEE, Graz, 2014).

[53] I. Rea, A. Lamberti, I. Rendina, G. Coppola, M. Gioffrè, M. Iodice, M. Casalino, et al., "Fabrication and characterization of a porous silicon based microarray for label-free optical monitoring of biomolecular interactions," J. Appl. Phys. **107**, 014513 (2010).

[54] I. Rea, E. Orabona, A. Lamberti, I. Rendina, and L. De Stefano, "A microfluidics assisted porous silicon array for optical label-free biochemical sensing," Biomicrofluidics **5**, 034120 (2011).

[55] E. Orabona, I. Rea, I. Rendina, and L. De Stefano, "Numerical optimization of a microfluidic assisted microarray for the detection of biochemical interactions," Sensors **11**, 9658–9666 (2011).

[56] L. De Stefano, I. Rea, E. Orabona, and I. Rendina, "Microfluidics assisted biosensors for label-free optical monitoring of molecular interactions," Sensor. Actuat. B-Chem. **179**, 157–162 (2013).